La mer 30: 251–262, 1992
Société franco-japonaise d'océanographie, Tokyo

Volume and heat transports of the Kuroshio in the East China Sea in 1989

Yaochu YUAN*, Jilan SU* and Ziqin PAN*

Abstract: A modified inverse method is used to compute the Kuroshio in the East China Sea with hydrographic data and moored current meter records obtained during early summer and autumn in 1989. In this method the geostrophic assumption is not imposed. The vertical viscous term in the momentum equation as well as the vertical diffusion term in the conservative equation and the heat exchange at the surface are all considered. The computed volume transports at R_1 (PN) section are 35 and $31\times10^6 m^3/s$ during early summer and autumn, respectively, in 1989. The heat transports are 2.50 and $2.29\times10^{15}W$ there during early summer and autumn, respectively, in 1989. About $1.29\times10^{13}W$ of heat is transferred into the ocean from atmosphere over the region of computation during early summer of 1989 and about $2.80\times10^{13}W$ of heat from the ocean to the atmosphere during autumn of 1989. A countercurrent is present in the deep layer during both periods. The total volume transport of the Taiwan Warm Current is about $1.5\times10^6 m^3/s$.

1. Introduction

Most of the previous studies on the volume transport of the Kuroshio in the East China Sea were based on the dynamic method (e.g. GUAN, 1982 and 1988; NISHIZAWA *et al.*, 1982). The level of no motion is normally set at 7 MPa. The annual mean volume transport thus computed for the Kuroshio through the PN section in the East China Sea is usually around $20\times10^6 m^3/s$. (The position of the PN section is the same as section R_1 shown in Fig. 1(a)). Recently YUAN, ENDOH and ISHIZAKI (1991) and YUAN, SU and PAN (1991) applied the inverse method to compute the current structure and volume transport of the Kuroshio in the East China Sea. Their results showed that the conservation of mass is not satisfied by the dynamic method and approximately satisfied by the inverse method. In these studies the geostrophic relation was assumed, as is the normal practice for inverse method (WUNSCH, 1978). However, the geostrophic assumption is not always valid (YUAN *et al.*, 1986).

In this paper, a modified inverse method is proposed to compute the current structure of the Kuroshio in the East China Sea. The hydrographic data and moored current meter records used were obtained in early summer and autumn of 1989.

* Second Institute of Oceanography, SOA, P. O. Box 1207, Hangzhou 310012, China

2. Modified inverse method

Both the vertical friction term in the momentum equation and the vertical diffusion term in the density equation are kept in our modified inverse method. In addition, the heat flux through the sea surface is also considered. In the following we shall discuss the rationale and results.

1) The vertical friction term in momentum equation is kept because the East China Sea shelf is shallow. If we further take the rigid-lid assumption, the boundary conditions at the surface are then

$$\rho_0 A_z \frac{\partial u}{\partial z}=\tau_x,\ \rho_0 A_z \frac{\partial v}{\partial z}=\tau_y$$
$$w=0 \qquad (1)$$

where the x-axis is parallel to hydrographic section, the y-axis normal to the section, and the z-axis upward. $\tau\ (\tau_x, \tau_y)$ is the wind stress vector, u and v are the horizontal velocity components, and w the vertical velocity component.

No-slip boundary condition is specified at the

bottom, i.e., at $z=-H(x, y)$

$$u=v=w=0 \tag{2}$$

For constant A_z an approximate expression for the horizontal velocity can be found (see YUAN *et al.*, 1986). For example, the v component can be written approximately as

$$v=v_\tau+v_G+v_B \tag{3}$$

v_τ is the surface Ekman velocity component subject to the wind stress τ, v_G is the geostrophic velocity, i,e.,

$$v_G = b_0-\frac{g}{f\rho_0}\int_z^{z_0}\frac{\partial \rho}{\partial x}\,dz \tag{4}$$

where b_0 is the value of v_G at the reference level z_0 and is an unknown to be computed. v_B is the bottom Ekman velocity components. If the pressure gradient is mainly in the along-section direction, i.e., $|\partial p/\partial x| \gg |\partial p/\partial y|$, then v_B can be expressed simply as (YUAN at al., 1986):

$$\begin{aligned} v_B=&-2\,(\cos aH \operatorname{ch} aH \cos az \operatorname{ch} az \\ &+\sin aH\, sh\, aH \sin az \operatorname{sh} az)\; v_G \\ &/(\cos aH+\operatorname{ch} aH) \end{aligned} \tag{5}$$

in which

$$a=(f/2A_z)^{1/2}$$

2) SARKISYAN (1977) has shown that in either the density or salt equation, the convection terms are of dominant importance and the horizontal diffusion terms are smaller than the vertical diffusion term. If we keep all convection terms and the vertical diffusion term in the density and salt equation but drop the horizontal diffusion terms, then the following equations for the j th layer of box i can be obtained:

$$\begin{aligned} &\iint_{A_{i,j}} \rho\,(x,y,z)\,C(x,y,z)\,v\,(x,y,z)\,\delta_{i,j}\,dA_{i,j} \\ &=C_j\rho_j w_j\delta_j A_j-C_{j-1}\rho_{j-1}w_{j-1}\delta_{j-1}A_{j-1} \\ &\quad+K_v\Big[\iint_{A_j}\frac{\partial(\rho C)}{\partial z}\,dA_j-\iint_{A_{j-1}}\frac{\partial(\rho C)}{\partial z}\,dA_{j-1}\Big] \end{aligned} \tag{6}$$

K_v is the vertical diffusion coefficient, assumed to be constant, $\delta_{i,j}$ (δ_j, δ_{j-1}) takes the value of 1 for flow into the box and -1 for flow out of the box. When $C(x, y, z)=1$, Eqn. (6) represents the mass conservation, and when $C(x, y, z)=S(x, y, z)$. Eqn. (6) represents the salt conservation equation. $A_{i,j}$ is the lateral face for the j th layer of box i, A_{j-1} and A_j are the projection of the upper and bottom faces of the j th layer of box i on the horizontal plane, respectively. In the standard inverse method, all terms on the left hand side of Eqn. (6), i.e. the vertical fluxes in the conservation equation, are neglected (e.g. WUNSCH, 1978). However, as we shall see later, the vertical fluxes due to the surface and bottom Ekman layer effect can not be neglected in the deep layer.

From Eqns. (3)–(6), we can write the following matrix

$$Ab=\Gamma \tag{7}$$

where b is $N\times 1$ matrices, and unknowns (b_0, w_j), A and Γ can be computed from the hydrographic and wind data.

3) Considering that the heat flux q_e at the sea surface is unknown, the following constraints are imposed, i.e.,

$$q_{e,1}\leq q_e\leq q_{e,2} \tag{8}$$

where $q_{e,1}$ and $q_{e,2}$ are, respectively, minimum and maximum statistical monthly average values in the survey area. We take the values of $q_{e,1}$ and $q_{e,2}$ as given by the Institutes of Oceanography and Geography of the Academia Sinica in 1977. q_e is an unknown to be computed. Positive value of q_e indicates heat transfer from the ocean to the atmosphere, and negative value of q_e indicates the heat transfer from the atmosphere to the ocean.

Eqn. (7) is solved with the inequalities (8) imposed. This is a mathematical problem of quadratic programing. Details of the computation of the problem can be found in WUNSCH (1982). If Eqn. (7) is solved without the inequalities (8), it is a linear programing problem (e.g. FIADEIRO and VERONIS, 1982; YUAN *et al.*, 1990).

On the choice of an optimum reference level, we use the FIADEIRO and VERONIS's method

(1982). Each box is divided into K layers. The geostrophic velocity v relative to z_0 level is given by

$$v=-\frac{g}{f\rho_0}\int_{z_0}^{z}\frac{\partial\rho}{\partial x}\,dz \tag{9}$$

We difine

$$T_{j,e}=\oint\int_{z_{j+1}}^{z_j} v\,dz\,dx, \quad (e=1,2;\cdot;M) \tag{10}$$

and

$$T_0^2=\sum_{e=1}^{M}\sum_{j=1}^{K}T_{j,e}^2 \tag{11}$$

where M is the number of boxes. A good choice for a reference level z_0 is such that T_0^2 is the minimum. If $z_0>H$(the water depth) at some stations, the reference levels at these stations are reset to be H.

The volume transport (VT) Q_m is defined as

$$Q_m=\int_L dx\int_{-H}^{0} v\,dz \tag{12}$$

where L is the width of the section, Substituting Eqn. (3) into Eqn. (12), we obtain

$$Q_m=Q_{m,\tau},+Q_{m,G}+Q_{m,B} \tag{13}$$

where

$$\begin{aligned} Q_{m,\tau}&=\int_L dx\int_{-H}^{0} v_\tau\,dz\\ Q_{m,\tau}&=\int_L dx\int_{-H}^{0} v_G\,dz\\ Q_{m,\tau}&=\int_L dx\int_{-H}^{0} v_B\,dz \end{aligned} \tag{14}$$

$Q_{m,G}$ is the geostrophic transport, $Q_{m,\tau}$, is the surface Ekman transport due to the surface wind stress and $Q_{m,B}$ is the bottom Ekman transport due to the bottom friction.

The heat transport Q_t due to ocean currents across a section S is well approximated by

$$Q_t=\iint_s \rho\,C_p T\vec{v}\cdot\vec{n}ds \tag{15}$$

Let

$$\left.\begin{aligned} \vec{v}&=\bar{\vec{v}}+\vec{v}'\\ T&=\bar{T}+T' \end{aligned}\right\} \tag{16}$$

in which $\bar{\vec{v}}$ and $\bar{T}$ are the depth-averaged velocity and temperature, respectively, $\vec{v}'$ is the baroclinic velocity component and T' is the deviations from the average temperature. Then Eqn. (2) becomes

$$Q_t=\iint_s \rho\,C_p\bar{T}\bar{\vec{v}}\cdot\vec{n}dzdx+\iint_s \rho\,C_p T'\vec{v}'\cdot\vec{n}dzdx \tag{17}$$

The heat transport (HT) components can be now divided into two parts, namely, the barotropic and baroclinic components.

3. Data and parameters

In this study both the hydrographic data and moored current meter data are used. During the early summer cruise in 1989, a short-term (5 May–7 May) moored station M_2 was located on section S_5 (Fig. 1.(a)) at 241 m water depth. One current meter was set at 80 m depth and the observed average volocity is 8.2 cm/s and 24° clockwise from north. During the autumn cruise in 1989, a moored station M_1 was located on section S_2 (Fig. 1.(b)) at 100 m water depth. Two current meters were set at 40 and 80 m depths, and their observation period was from Oct. 11 to Oct, 22. The time-averages of the observed velocities at 40 m and 80 m depths were (14.6 cm/s, 31°) and (13.5 cm/s, 8°), respectively. For this computation, only the observed velocity at 80 m level is used as a known value of velocity at the 80 m reference level in Eqn. (7).

Both the vertical diffusion coefficient K_v and vertical eddy coefficient A_z are assumed to be constant. We have experimented with different values of these coefficients, namely, A_z=50 and 100 cm²/s and K_v=1 and 10 cm²/s.

The average wind direction and speed as observed on board R/V Shijian were 223° (SW) and 6.5 m/s during the early summer cruies of 1989 and 43.7° (NE) and 9.3 m/s during the autumn cruise of 1989, respectively. Because of the lack of accurate wind data, a steady uniform wind field for each cruise with the above respective average values is assumed.

To compare the effects of the vertical viscous terms and the vertical diffusion terms we try two values of vertical eddy coefficient A_z (50 and 100cm²/s) and two values of vertical

diffusion coefficient K_v (1 and 10cm^2/s). The values of q_{e1} and q_{e2} are taken to be, respectively, -1.7 and 0.8×10^3 J/cm^2 d for the early summer cruise and 1.3 and 2.1×10^3J/cm^2 d for the autumn cruise (see Institute of Oceanography and Geography, 1977). For comparison we have also carried out computations without imposing the inequality constraints.

4. Numerical experiments

Figures 1. (a), (b) show the bathymetry, hydrograhic sections and computation boxes for the early summer and autumn, respectively, in 1989. The computation points are at the midpoints between neighboring hydrographic stations. All boundary sections of the computation boxes are divided into layers according to isopyncal $\sigma_{t,p}$ values of 24, 27, 30 and 33. For example at the section S_5 during early summer cruise, the depths of $\sigma_{t,p}=24$, 27, 30 and 33 levels lie between 30 to 120 m, 250 to 350 m, 650 to 700 m and around 1250 m, respectively (Fig. 2)

To compare the computation results for different physical parameters we carried out a number of experiments. The symbol CA-i-j denotes a particular experiment. i=1,2 denote the early summer and autumn cruises, respectively, in 1989. j=1 indicates that the inequality constraints are not imposed and j=2 the inequality constraints are imposed.

From Eqns (9)–(11), the values of T_0^2 for different reference levels are computed. For the early summer data the minimum value of T_0^2 is found at H, the water depth, and thus the reference level is taken to be the water depth H. For the autumn data the minimum of T_0^2 is at z_0 =600 m level. However, since the value of T_0^2 at $z_0=H$ is close to the minimum value, in order to compare the results of the two data sets, the reference level for the autumn data is also taken at the water depth.

For the two values of vertical diffusion coefficient K_v(1 and 10 cm^2/s), the respective computed volume transports differ by less than 4%. The computed volume transport for different values of vertical eddy coefficient A_z(50 and 100 cm^2/s) changes less. In the following discussions the results are all based on $A_z=100$ cm^2/s and $K_v=10$ cm^2/s.

Because of the shallowness of the surface layer

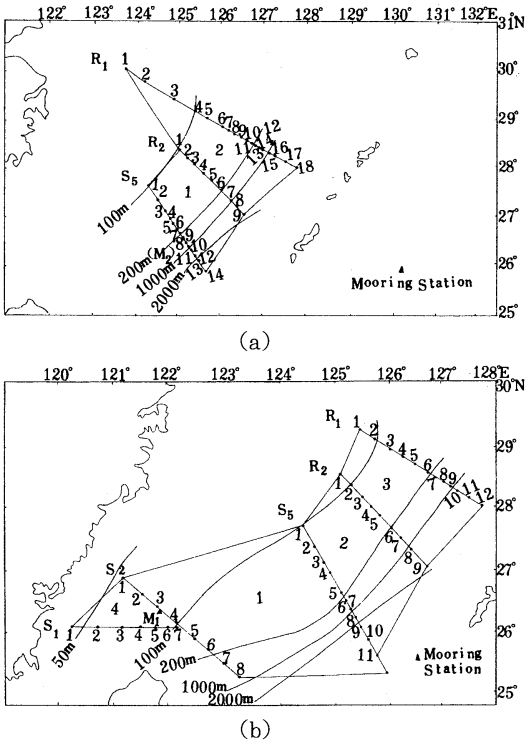

Fig. 1. Sketch of bottom topography (in meters), and locations of hydrographic and mooring stations and computation boxes (a) for early summer (May and June) of 1989 and (b) for autumn (October) of 1989.

and also the lack of surface boundary conditions for salt, consideration of the salt convection-diffusion equation for the surface layer or not usually has no significant effect on the computation results. Our experiments confirm it, too. It is found that the two cases where the salt equation for the surface layer is considered or not result in relative changes of volume transports by less than 0.1%. Hence all results presented in the following discussions are based on consideration of the salt convection-diffussion equations for all layers except the surface layer.

On the numerical computation of this method, we discuss the following questions.

Table 1 lists the balances of the volume, salt and heat transports by the modified inverse method and those by the dynamic method, respectively. For meaningful comparison, the level of no motion for the dynamic method is also taken to be the water depth H. Box-1 is bounded by sections S_5 and R_2 of the early

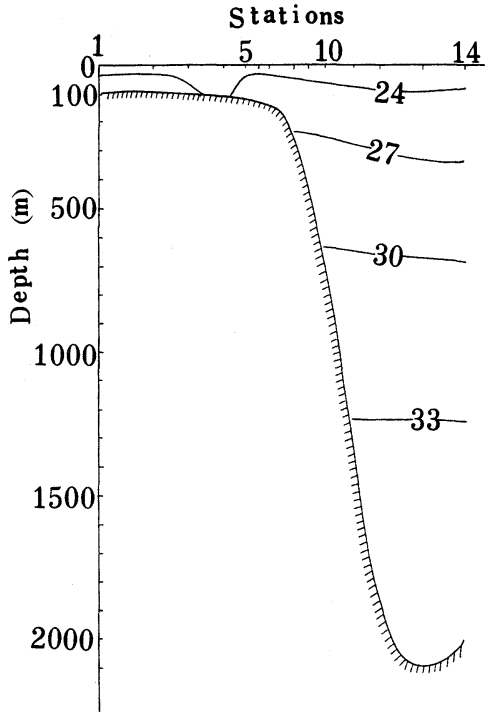

Fig. 2. Isopycnal levels along section S_5 for early summer (May and June) of 1989.

summer observation in 1989 (Fig. 1(a)) and box-2 is bounded by the same sections of the autumn observation in 1989 (Fig. 1(b)). Table 1 indicates that (1) for the dynamic method conservations of volume, salt and heat transport are all not satisfied; (2) conservations of both volume and salt are satisfied approximately for CA-i-1 and CA-i-2.

According to the data given by Institute of Oceanography and Geography of Academia Sinica (1977), the bounds of the magnitude of the heat flux at the sea surface for boxes 1 and 2 is 10^{12}~10^{13}W. For case CA-i-1 which dose not impose the inequalities (8), the unbalanced amount of the heat flux is of the order of 10^{13}~10^{14}W (Table 1), much larger than the bounds of the heat flux at the sea surface given above. This means that the heat flux at the sea surface can not be obtained by case CA-i-1, and the inequality constraints. Egn. (8) are necessary for obtaining approximately the heat flux at the sea surface.

Table 1. The balance of the volume, salt and heat transports in box-1 during early summer of 1989 and box-2 during autumn of 1989.

Box	Method	$\triangle_m$	$\triangle_s/34.5‰$	$\triangle_t$
	Dynamic method*	−1.72	−1.69	−8.34
Box-1	CA-1-1	−0.02	0.00	−5.91
	CA-1-2	−0.02	−0.01	−0.72
	Dynamic method*	−3.78	−3.85	−29.51
Box-2	CA-2-1	0.04	−0.00	−12.85
	CA-2-2	0.04	−0.03	0.61

Note

*: The level of no motion is set at the water depth H.

$\triangle_m$: balance of volume transport into the box (positive into the box, units: $10^6 m^3/s$).

$\triangle_s$: balance of salt transport into the box (positive into the box, units of $\triangle_s/34.5‰$: $10^6 m^3/s$)

$\triangle_t$: balance of heat transport into the box (positive into the box, units: 10^{13}W).

In the following we compare the results obtained with the modified method (CA-i-1 and CA-i-2) and the dynamic method.

Table 2 shows that the difference in VT obtained by the modified method (CA-i-1 and CA-i-2) and dynamic method is not large. However, the differences in VT at the lateral sections west of either box-1 or box-2 is large. For example, the VT through the lateral section west of box-1 is $0.6\times10^6 m^3/s$ for case CA-1-2 (Fig. 5), but $0.25\times10^6 m^3/s$ with the dynamic method. It is worthy of note that the Ekman transport at the section is maximum when the wind direction is parallel to this section. During early summer of 1989, the angle between the orientation of section S_5 (R_2 and R_1) and the wind direction is large. Thus the wind stress has little effect on the VT of the Kuroshio. However it has important effects on the VT at the lateral sections of the boxes, especially the lateral section on the shallow shelf. Table 3 shows that there are some differences in VT obtained with the modified method (CA-i-1 and CA-i-2) and dynamic method for the autumn observation of 1989.

To see the effect of the imposed surface heat flux inequality we compare the results of CA-i-1 and CA-i-2 (Tables 2 and 3). The relative changes of volume transport (VT) and heat transport (HT) between CA-1-1 and CA-1-2 are both less than 2% for the data of early summer of 1989 (Table 2). For the data of autumn of

Table 2. Comparison of the VT ($10^6 m^3/s$) and HT($10^{15}W$) at sections obtained with the dynamic method and the modified inverse method (CA-1-1 and CA-1-2) during early summer of 1989.

Method	section S_5		section R_2		section R_1	
	VT	HT	VT	HT	VT	HT
Dynamic method*	29.2		28.8		36.1	
CA-1-1	30.3	2.28	29.1	2.09	35.0	2.52
CA-1-2	30.4	2.31	28.7	2.06	34.6	2.50

*: The level of on motion is set at the water depth H.

Table 3. Comparison of the VT($10^6 m^3/s$) and HT($10^{15}W$) at sections obtained with the dynamic method and the modified inverse method (CA-2-1 and CA-2-2) during autumn of 1989.

Method	section S_5		section S_5		section R_2		section R_1	
	VT	HT	VT	HT	HT	HT	HT	HT
Dynamic method*	11.4		33.0		21.2		30.6	
CA-2-1	15.3	1.43	22.1	2.30	18.3	1.72	30.5	2.24
CA-2-2	16.0	1.51	29.2	2.53	17.6	1.56	31.0	2.29

*: The level of on motion is set at the water depth H.

Table 4. The horizontal and vertical volume transports through the section or the face in each layer of box-1 for early summer in 1989

layer	section S_5	$(EL)_1$	section R_2	$(WL)_1$	$(VVT)_j$	$\triangle_j$
1st	6.94	−0.73	− 6.73	0.25	0 0.24	−0.03
2nd	15.40	−2.81	−11.86	0.39	−0.24 −0.87	0.01
3rd	7.59	−0.75	− 8.55	0	0.87 0.85	0.01
4th	0.42	1.28	− 1.30	0	−0.85 0.45	−0.00
5th	0.05	0.64	− 0.25	0	−0.45 0	−0.01
total	30.40	−2.37	−28.69	0.64	0	−0.02

Note
$(WL)_1$: the western lateral section of box-1
$(EL)_1$: the eastern lateral section of box-1
$(VVT)_j$: the upper and lower numbers denote the vertical volume transports at the upper and lower faces of the j-th layer, respectively.
$\triangle_j$: the balance of volume transport into the j-th of box-1. (positive into the layer, units; $10^6 m^3/s$).

1989, however, although relative changes of both VT and HT between CA-2-1 and CA-2-2 are small for section R_1, large relative change of HT reaches 9% at both sections R_2 and S_5 (Table 3). At section S_5 the relative change of VT between CA-2-1 and CA-2-2 is as high as 24%. This indicates that the data of autumn of 1989 is probably noisier than the data of early summer of 1989. In the following, our discussions will concentrate mainly on results with inequality constraints, (8) imposed.

Now we discuss the horizontal and vertical

Table 5. The horizontal and vertical volume transports through the section or the face in each layer of box-2 for the early summer in 1989

layer	section PN	$(EL)_2$	section S_5	$(WL)_2$	$(VVT)_j$	$\triangle_j$
1st	− 7.68	1.22	6.73	0.12	0 −0.43	−0.04
2nd	−17.34	2.84	11.86	0.42	0.43 1.81	0.02
3rd	− 9.01	0.74	8.55	0	−1.81 1.53	0.00
4th	− 0.65	0.63	1.30	0	−1.53 0.25	0.00
5th	0	0	0.25	0	−0.25 0	0.00
total	−34.68	5.43	28.69	0.54	0	−0.02

Note
$(WL)_2$: the western lateral section of box-2
$(EL)_2$: the eastern lateral section of box-2
$(VVT)_j$: the upper and lower numbers denote the vertical volume transports at the upper and lower faces of the j-th layer, respectively.
$\triangle_j$: The balance of volume transport into the j-th of box-2. (positive into the layer, units; $10^6 m^3/s$).

volume transport in each layer using the early summer observation as the example. Tables 4 and 5 show that over 95% of the VT of the Kuroshio is in the 1st, 2nd and 3rd layers, i.e., above the 700 m level. Comparing the magnitude of the horizontal VT of the Kuroshio with the vertical volume transport (VVT), the magnitude of the VVT is much less then the Kuroshio VT in the 1st, 2nd and 3rd layers. However, they are same order in the 4th and 5th layers. Finally, the horizontal volume transport through the western lateral section of box, i.e. the section on the shallow shelf in the East China Sea, is of the same order at the vertical volume transport (Tables 4, 5 and Fig. 5).

During the autumn of 1989 the moored station M_1 has two observation depths, 40 and 80 m. The observed average velocity at 80 m is used for computation. The computed velocity at the 40 m level of the same station has a 16.1 cm/s component normal to section S_2, which agree well with the observed value of 14.5 cm/s.

5. Velocity and volume transport distribution during early summer (May-June) of 1989

5.1 Velocity distribution

Fig.3 shows the velocity distribution at section S_5 for case CA-1-2. The core of the Kuroshio is located over the slope. The maximum velocity is found at the 75 m level with a magnitude of 111 cm/s. As found in previous studies (e.g. YUAN and SU, 1988), in the deep layer, the axis of the Kuroshio seems to be further eastward as it flows northward. There are two countercurrents in the Kuroshio region. One is at the bottom layer near the shelf break and its maximum speed is greater than 30 cm/s. The other is below 800 m level over the lower part of the continental slope, but its speed is smaller than 2 cm/s.

At section R_2, the Kuroshio core is located also over the shelf break. The 100 cm/s isotach reaches as deep as 125 m and the maximum velocity is found at 50 m with a magnitude of 129 cm/s. There is no countercurrent below the Kuroshio. However, there is a countercurrent over the shelf at the bottom layer near the shelf break.

The Kuroshio speed at section R_1 is greater than at other sections, probably due to both the shallow water depth there and the merging of currents from the eastern lateral section of box-2 (Fig. 5). Its maximum velocity (about 149

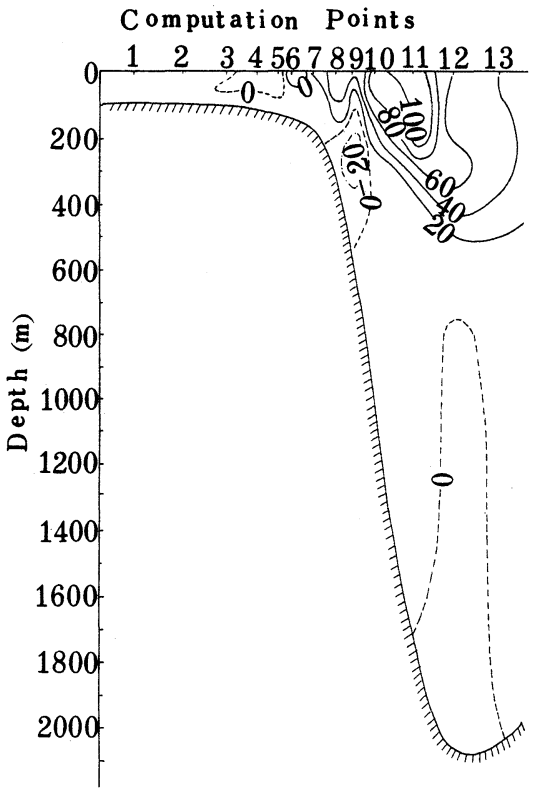

Fig. 3. The velocity distribution at section S_5 during early summer of 1989 for case CA-1-2. (units: cm/s)

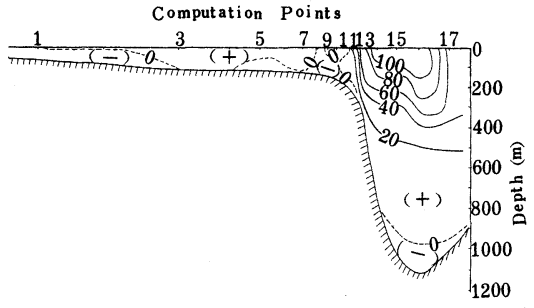

Fig. 4. The velocity distribution at section R_1 during early summer of 1989 for case CA-1-2. (units: cm/s)

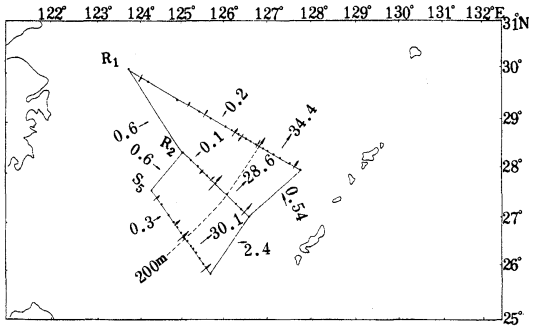

Fig. 5. Volume transport distribution in the computational region during early summer of 1989 for case CA-1-2. (units:$10^6 m^3/s$)

cm/s) is found at the surface (Fig. 4). At the 200 and 400 m levels the maximum velocities are 90 and 39 cm/s, respectively, and their positions are both located east of the surface maximum. Landward of the front there is a southward current on the shelf and its maximum velocity is about 20 cm/s. Under the Kuroshio there is a very weak southward current at the bottom of the trough.

5.2 Volume transport distribution

There is a cyclonic gyre or a southward current west of Kuroshio (Fig. 4). The Kuroshio width is more than 100 km. The volume transport (VT) of the Kuroshio at sections S_5 and R_1 is about 30 and $35 \times 10^6 m^3/s$, respectively, greater than the computed Kuroshio VT during early summer of 1988 (YUAN, SU and PAN., 1991). The intrusion of the Kuroshio water over the shelf at section R_5 is further to the west than that at sections S_5 and R_1 (Fig. 5). This is in agreement with the position of Kuroshio axis (Figs. 3 and 4).

Finally, as previous studies (SU and PAN, 1987; YUAN *et al*, 1987) pointed out, there is the northeastward current over the East China Sea shelf, which was called Taiwan Warm Current, and it may be considered as being a combination of two current systems, an inshore branch and an offshore branch. The VT of Taiwan Warm Current (TWC) which also flows through the computational region is about $1.5 \times 10^6 m^3/s$, i.e. $0.6+0.6+0.3=1.5(10^6 m^3/s)$(Fig. 5). When this shelf current flows northeastward through section R_1, most of it has a tendency to converge to the shelf break, similar to the findings of previous studies (e.g. YUAN and SU, 1988).

6. Velocity and volume transport distributions during autumn (October) of 1989

6.1 Velocity distribution

The velocities at section S_2 during the 1989 autumn cruise are not very large (Fig. 6). There

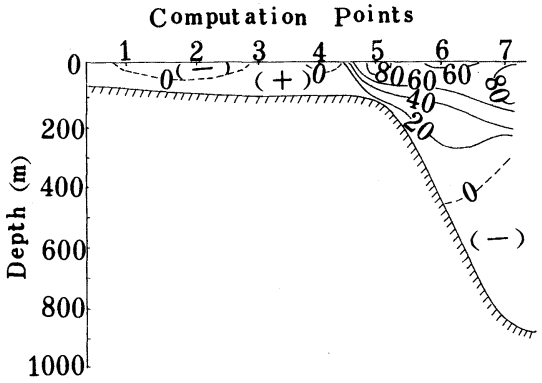

Fig. 6. The velocity distribution at section S_2 during autumn of 1989 for CA-2-2. (units:cm/s)

are two cores at section S_2. One is located at the shelf break. Its maximum velocity is about 86.4 cm/s at 25 m level. The other is located over the lower part of the slope and the velocities from 25 to 125 m levels are all greater than 80 cm/s. Below the latter core there is a countercurrent and its maximum speed is greater than 10 cm/s. At the shallow end of shelf there is a southward current in the surface layer, probably due to the strong northeast winds, but near the bottom the current is still northward (Fig. 6).

Fig. 7 shows that the core of Kuroshio at section S_5 is located close to the shelf break and the Kuroshio front is evident. Its maximum velocity is greater than 150 cm/s at the 25 m level. There is a countercurrent occupying most part of the Okinawa Trough below 600 m. This current is rather strong; for example, its velocities at the 1000 and 1500 m levels are greater than 9 and 4 cm/s, respectively. This countercurrent extends back to section R_2 (Fig. 8). Its strength at section R_2 is even strong. Its maximum speed is greater than 22 cm/s at 800 m level, and at 1000 m level its velocity is still greater than 15 cm /s. Furthermore, the core of this countercurrent is closer to the continental slope than it is at section S_5. Consistent with this, the core of the Kuroshio at section R_2 is now located over the shelf break (Fig. 8). The maximum velocity of the Kuroshio is about 90 cm/s at the 25 m level.

Like the early summer case, the Kuroshio Current speed at section R_1 is also greater than at other sections (Fig. 9), probably because of the shallow water depth at section R_1 and the merging of currents from the eastern lateral

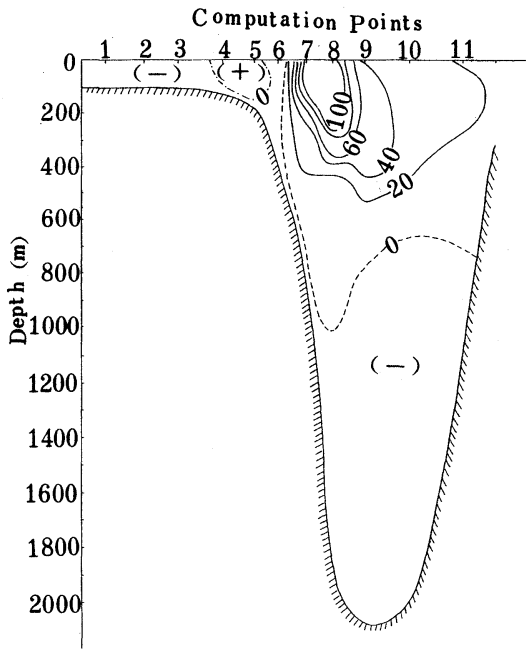

Fig. 7. The velocity distribution at section S_5 during autumn of 1989 for case CA-2-2. (units: cm/s).

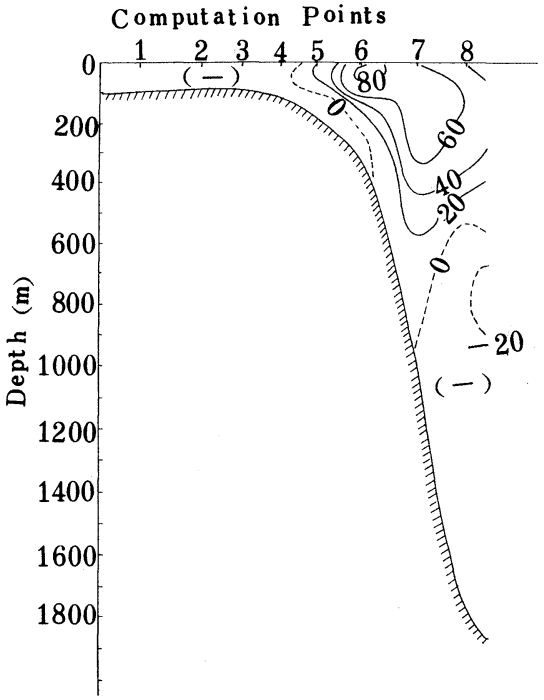

Fig. 8. The velocity distribution at section R_2 during autumn of 1989 for case CA-2-2. (units: cm/s)

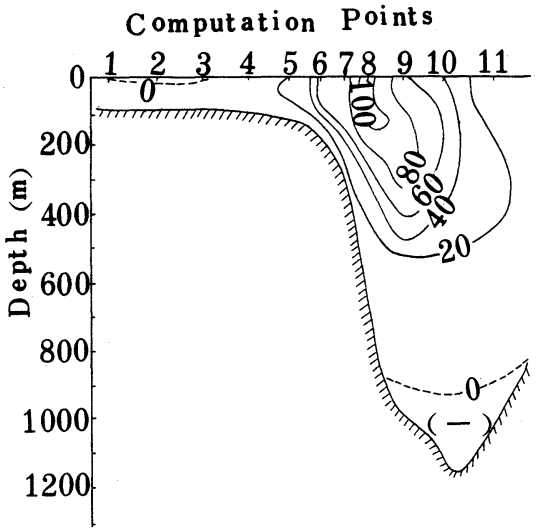

Fig. 9. The velocity distribution at section R_1 during autumn of 1989 for case CA-2-2. (units: cm/s)

section of box-3 (Fig. 10). Its maximum velocity is about 133 cm/s at 25 m level at point 8 of R_1. There is a countercurrent below 950 m level, but its velocity is smaller than at other sections.

6.2 Volume transport distribution

Fig. 10 shows the distribution of volume transport in the computational region during autumn of 1989 for case CA-2-2. The volume transport through section R_1 is about $30 \times 10^6 m^3/s$. Its VT is larger than during the same seasons of 1987 and 1988. However, it is less than during early summer of 1989 (Fig. 5). The countercurrent during autumn of 1989 is rather strong. Its VT is around $3 \times 10^6 m^3/s$ at section R_2 and $4 \times 10^6 m^3/s$ at section S_5. However, the volume transport of the countercurrent at sections R_2 and S_5 for CA-2-1 are 4 and $7.5 \times 10^6 m^3/s$, respectively. Thus, the difference of the computed countercurrent VT between CA-2-1 and CA-2-2 is large for section S_5. We shall comment on this matter later in this paper.

Fig. 10 also shows that there is a cyclonic gyre on the shelf north of Taiwan. The temperature distribution indicates that it is a cold gyre. Fig. 10 also shows that the total VT of TWC which flows into this computational region is about $1.5 \times 10^6 cm^3/s$.

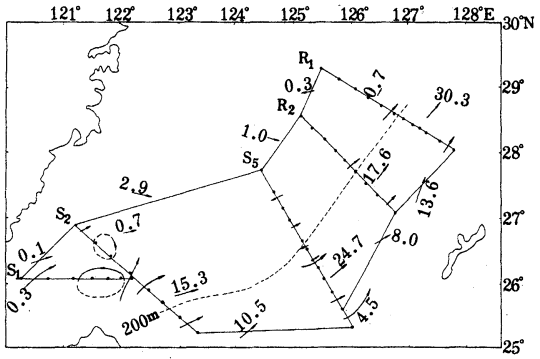

Fig. 10. Volume transport distribution in the computational region during autumn of 1989 for case CA-2-2. (units:$10^6 m^3/s$).

7. Heat transport

Table 6 lists the computed VT and HT of the Kuroshio through section R_1 for the early summer cruise and sections R_1 and S_5 for the autumn cruise. Other sections covered only parts of the Kuroshio and their results are not listed. For comparison the VT and HT of the Gulf Stream (Hall and Bryden, 1982) are also listed in Table 6. The symbols $Q_{t,1}$ and $Q_{t,2}$ denote the barotropic and baroclinic components of heat transport and the symbol $\tilde{T}$ is defined as the average temperature:

$$\tilde{T} = Q_t (\rho C_p Q_m)^{-1} \tag{18}$$

In general, the barotropic component of the heat transport seems to be larger than the baroclinic component for either the Kuroshio or the Gulf Stream, except for the Kuroshio at section S_5 during autumn of 1989 when the baroclinic component is higher than the barotropic component.

The computed results for case CA-i-2 show that during early summer of 1989 the heat transfer is from the atmosphere to the ocean for boxes 1 and 2 and their values are 7.2 and $5.7 \times 10^{12} W$, respectively, totaling $1.29 \times 10^{13} W$. During autumn of 1989 the total heat transfer is from the ocean to the atmosphere and it is about $2.80 \times 10^{13} W$. The values of these heat exchanges at the sea surface are less than 0.5% of the HT of the Kuroshio through each section. This means that high quality hydrographic data is necessary to obtain reliable heat flux values at the sea surface.

Table 6. The comparison of VT (units:10^6m^3/s) and HT(units:10^{15}W) between the Kuroshio (CA-i-2) and Gulf Stream

Current system	time	section	VT	HT	$\tilde{T}$(℃)	$Q_{t,1}$	$Q_{t,2}$
Kuroshio	early summer of 1989	R_1	34.6	2.50	17.64	1.60	0.90
Kuroshio	autumn of 1989	R_1	31.0	2.29	18.11	1.71	0.58
Kuroshio	autumn of 1989	S_5	29.2	2.53	21.20	1.17	1.36
Gulf Stream*	annual mean in 1973	Florida Straits	29.5	2.38	19.71	1.88	0.50

* From Hall and Bryden, (1982).

To see the effect of the inequality constraints (8) on the computed heat flux at the sea surface, we compare case CA-i-2 with case CA-i-1 again. The computed results of case CA-1-1 show that during early summer of 1989 there is 5.65×10^{13} W of heat transferred into the ocean from the atmosphere over the computational region, about 8 times larger than the computed value for case CA-1-2. The difference of the computed air-sea heat fluxes between CA-2-1 and CA-2-2 during autumn of 1989 is even larger. For example, the heat transfer from the ocean to the atmosphere through the sea surface of box-1 is 1.03×10^{13}W for case CA-2-2, but 38.02×10^{13}W for case CA-2-1 and in opposite direction from the atmosphere to the ocean. This seems to indicate that the quality of the 1989 autumn cruise data is not so good as the 1989 early summer cruise data and the inequality constraints, (8) is necessary for the inverse computation.

8. Summary

A modified inverse method is used to compute the Kuroshio in the East China Sea, based on the hydrographic data and moored current meter records obtained during both early summer and autumn of 1989. It is found that:

1) In general, on a broad shallow shelf the surface Ekman velocity component due to the wind stress can not be neglected; thus our modified inverse method is useful in shallow seas. When the quality of the hydrographic data is poor, to obtain the heat flux at the sea surface, the inequality constraints at the sea surface. (8) seems to be needed.

2) The vertical volume transport (VVT) has less effect on the total volume transport of the Kuroshio. However, the VVT can not be neglected in the deep layer. The VVT is of the same order of magnitude as the horizontal volume transport through the west lateral section of box, i.e. the section on the shallow shelf in the East China Sea.

3) The volume transports at section R_1(PN) are 35 and 31×10^6m^3/s during early summer and autumn, respectively, in 1989. The heat transports at R_1 (PN) section are 2.50 and 2.29×10^{15} W during early summer and autumn, respectively, in 1989.

4) The Kuroshio Current speed at section R_1 is greater than at other sections, probably due to both the shallow water depth at section R_1 and the merging of currents from the eastern lateral section of box-2 (Fig. 5) or box-3 (Fig. 10).

5) A countercurrent is present in the deep layer during both cruises of 1989. It is stronger during autumn of 1989.

6) The VT of TWC flowing into this computational region is about 1.5×10^6m^3/s during both cruises of 1989.

7) During both cruises of 1989 the barotropic components of HT is in general larger than the corresponding baroclinic components. About 1.29×10^{13}W of heat is transferred into the ocean from the atmosphere over the computational region during early summer of 1989 and about 2.80×10^{13}W of heat from the ocean to the atmosphere over the computational region during autumn of 1989.

References

FIADEIRO, M.E and G. VERONIS (1982): On the determination of absolute velocities in the ocean. J. Mar. Res., 40, Suppl., 159–182.

GUAN, BINGXIAN (1982): Analysis of the variations of volume transport of Kuroshio in the East China Sea. *In*: Proc. Japan-China Ocean Study Symp.,K. HISHIDA *et al.*, eds, Tokai Univ. Press, 118–137.

GUAN, BINGXIAN (1988): Major feature and variability of the Kuroshio in the East China Sea. Chinese. J. Oceanol. Limnol., **6**, 35–48.

HALL, M.M. and H.L. BRYDEN (1982): Direct

estimates and mechanisms of ocean heat transport. Deep-Sea Res., **29**, 339–359.

Institute of Oceanography and Geography, Academia Sinica (1977): The Atlas of heat balance at the sea surface in the Bohai Sea, Yellow Sea and East China Sea, Chinese Science Press, 160 pp.

NISHIZAWA , J., E. KAMIHIRA, K. KOMURA, R.KUMABE and M.MIYAZAKI (1982): Estimation of the Kuroshio mass transport flowing out of the East China Sea to the North Pacific. La mer, **20**, 37–40.

SARKISYAN, A.S. (1977): The diagnostic calculations of a large-scale oceanic circulation. *In*: The sea, vol.6, E.D.Goldberg *et al.*, eds, Wiley-Interscience Publication, 363–458.

SU, JILAN and PAN YUQIU (1987): On the shelf circulation north of Taiwan. Acta Oceanologica Sinica, **6** (Suppl. 1), 1–20.

WUNSCH, C. (1978): The general circulation of the North Atlantic west of 50° W determined from inverse methods. Rev. of Geophy. Space Phys., **16**, 583–620.

WUNSCH, C. and J.F. MINSTER (1982): Methods for Box Models and Ocean Circulation Tracers: Mathematical Programing and Nonlinear Inverse Theory. J. Geophy. Res., **87**C, 5647–5662.

YUAN, YAOCHU and SU JILAN (1988): The calculation of Kuroshio Current Structure in the East China Sea–Early Summer. Progress in Oceanography, **21**, 343–361.

YUAN, Y., M. ENDOH and H. ISHIZAKI (1991): The Study of the Kuroshio in the East China Sea and Currents East of the Ryukyu Islands. Acta Oceanologica Sinica, **10**, 373–391.

YUAN, YAOCHU, SU JILAN and PAN ZIQIN (1990) Calculation of the Kuroshio Current South of Japan During Dec., 1987–Jan., 1988. Proc. Investigation of Kuroshio (II), 256–266.

YUAN, YAOCHU, SU JILAN and PAN ZIQIN (1991): A Study of the Kuroshio in the East China Sea and the Currents East of the Ryukyu Islands in 1988. *In*: Oceanography of Asian Marginal Seas. K. TAKANO, ed. Elsevier Science Publishers, 305–319.

YUAN, YAOCHU, SU JILAN and XIA SONGYUN (1986): A diagnostic model of summer circulation on the northwest shelf of the East China Sea. Progress in Oceanography, **17**, 163–176.

YUAN, YAOCHU, SU JILAN and XIA SONGYUN (1987): Three dimensional diagnostic calculation of circulation over the East China Sea Shelf. Acta Oceanologica Sinica, **6** (Suppl. 1), 36–50.